AD-A190 091 MANAGEMENT ANDCCONTROL OF UNSTEADY AND TURBULENT FLOWS 1/1
(U) ILLINOIS INST OF TECH CHICAGO FLUID DYNAMICS
RESEARCH CENTER H M NAGIB ET AL. JUN 88
UNCLASSIFIED AFOSR-TR-88-0747 F49620-86-C-0133 F/G 20/4 NL

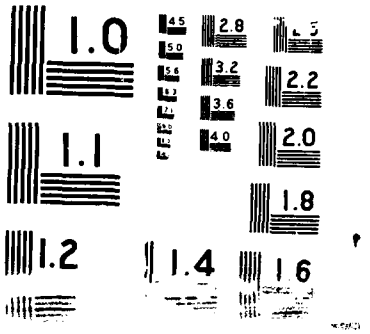
1.0
1.1
1.2
1.4
1.6
1.8
2.0
2.2
2.8
3.2
3.6
4.0
4.5
5.0
5.6

AFOSR-TR- 88-0747

TITLE: MANAGEMENT AND CONTROL OF UNSTEADY AND TURBULENT FLOWS

ANNUAL TECHNICAL REPORT

AFOSR Contract F49620-86-C-0133

PRINCIPAL INVESTIGATOR: Hassan M. Nagib

INVESTIGATORS: Mukund Acharya, Thomas C. Corke, Patrick H. Reisenthel, Candace E. Wark, John L. Way, and David R. Williams

JUNE 1988

Illinois Institute of Technology

Mechanical and Aerospace Engineering Department

Fluid Dynamics Research Center

Chicago, Illinois

UNCLASSIFIED

SECURITY CLASSIFICATION OF THIS PAGE

REPORT DOCUMENTATION PAGE

1a. REPORT SECURITY CLASSIFICATION unclassified	1b. RESTRICTIVE MARKINGS
2a. SECURITY CLASSIFICATION AUTHORITY	3. DISTRIBUTION/AVAILABILITY OF REPORT Approved for public release, distribution unlimited
2b. DECLASSIFICATION/DOWNGRADING SCHEDULE unlimited	
4. PERFORMING ORGANIZATION REPORT NUMBER(S)	5. MONITORING ORGANIZATION REPORT NUMBER(S) AFOSR-TR- 88-0747
6a. NAME OF PERFORMING ORGANIZATION Illinois Institute of Technology 6b. OFFICE SYMBOL (If applicable) IIT	7a. NAME OF MONITORING ORGANIZATION AFOSR
6c. ADDRESS (City, State and ZIP Code) MAE Dept. and FDRC 10 W. 32nd St Chicago, IL 60616	7b. ADDRESS (City, State and ZIP Code) AFOSR/NA Bolling Air Force Base Washington, DC 20332-6448
8a. NAME OF FUNDING/SPONSORING ORGANIZATION AFOSR 8b. OFFICE SYMBOL (If applicable) NA	9. PROCUREMENT INSTRUMENT IDENTIFICATION NUMBER F49620-86-C-0133
8c. ADDRESS (City, State and ZIP Code) AFOSR/NA Bolling Air Force Base Wasington, D.C. 20332-6448	10. SOURCE OF FUNDING NOS. PROGRAM ELEMENT NO. 61102F; PROJECT NO. 3484; TASK NO. A1; WORK UNIT NO.
11. TITLE (Include Security Classification) Management and Control of Unsteady and Turbulent Flows (unclassified)	
12. PERSONAL AUTHOR(S) H. Nagib, M. Acharya, T. Corke, P. Reisenthel, C. Wark, J. Way and D. Williams	
13a. TYPE OF REPORT Annual Technical 13b. TIME COVERED FROM ~~Oct 86~~ TO ~~Oct 87~~	14. DATE OF REPORT (Yr., Mo., Day) 1988, June 15. PAGE COUNT 14
16. SUPPLEMENTARY NOTATION	
17. COSATI CODES FIELD / GROUP / SUB. GR.	18. SUBJECT TERMS (Continue on reverse if necessary and identify by block number) Turbulence, Transition, Unsteady Flow, Separated Flow, Flow Control, Instrumentation.

19. ABSTRACT (Continue on reverse if necessary and identify by block number)

Progress in four areas of research has been achieved during the first year. I. Controlled Transitioning Boundary Layers: phase coupled plane TS waves and oblique waves are used to study various types of transition including detuned modes. II. Turbulent Boundary Layer Structure and Control: the structures responsible for the turbulence production in high Reynolds number boundary layers have been documented and manipulated. III. Management of Unsteady and Three-dimensional Flows: flows over airfoils, axisymmetric forebodies, vortex-wing interactions, and wing-body junctions, are examined with and without passive and active flow manipulators including zero-mass base bleed. IV. Scanning Laser Anemometry: a technique capable of mapping the flowfield in a plane has been developed.

20. DISTRIBUTION/AVAILABILITY OF ABSTRACT UNCLASSIFIED/UNLIMITED ☒ SAME AS RPT. ☐ DTIC USERS ☐	21. ABSTRACT SECURITY CLASSIFICATION Unclassified
22a. NAME OF RESPONSIBLE INDIVIDUAL Dr. James McMichael	22b. TELEPHONE NUMBER (Include Area Code) (202) 767-4936 22c. OFFICE SYMBOL AFOSR/NA

DD FORM 1473, 83 APR EDITION OF 1 JAN 73 IS OBSOLETE.

UNCLASSIFIED

SECURITY CLASSIFICATION OF THIS PAGE

I. CONTROLLED TRANSITIONING BOUNDARY LAYERS

SUMMARY:

The simultaneous generation of phase-coupled plane TS waves and oblique waves with respective wavenumbers $(\alpha_1,0)$ and (α_2,β_1), (α_2,β_2) are used to study the growth of three-dimensional disturbances in a Blasius boundary layer. This was accomplished using a computer controlled array of line heaters to produce spanwise-moving time-periodic velocity perturbations. Conditions for subharmonic resonance with a fundamental TS mode $(\alpha,0)$ and symmetric oblique modes $(\alpha/2,+\beta)$ and $(\alpha/2,-\beta)$ have been fully documented for different streamwise and spanwise wavenumbers. Of special interest was the growth of higher harmonic modes including $(3/2\alpha,\pm\beta)$, $(5/2\alpha,\pm\beta)$, $(\alpha,\pm2\beta)$ and $(0,\pm2\beta)$. Contrasted with these are nonlinear interactions produced by seeding nonfundamental/subharmonic modes. Comparisons point to the role of detuned modes as a mechanism for energy saturation and spectral filling associated with laminar to turbulent transition.

DISCUSSION:

In past experiments on the growth of 3-D modes in boundary layers by others, only plane TS modes had been directly forced. Any 3-D mode interactions were the result of indirect stochastic input from background disturbances. Because of the more difficult aspects of studying 3-D mode interactions and the potential problems of achieving spatial stationarity of three-dimensional features, we chose in our experiments (Corke and Mangano, 1987; and Corke and Dal-Ferro, 1987) to seed for the first time 3-D oblique waves of particular wave number content, simultaneously with plane TS waves. These modes were phase locked to produce resonant interactions of the type postulated by Craik (1971) and Herbert (1983).

The simultaneous 2-D and 3-D wave generation was accomplished using a array of 0.05mm diameter heating wires suspended at the height of the critical layer. These were periodically heated to introduce controlled perturbations through local changes in the air viscosity. The oblique waves were produced by using a spanwise array of individual heating wires. Each wire segment was individually controlled to produce periodic, laterally opposite, spanwise-moving velocity perturbations. By this approach, for an individual heating segment of length, s, a periodic time series input period, τ, and a radian phase shift between adjacent heating wires, ϕ, spatially propagating waves would be produced with a wave angle, θ, given by $\theta = \arctan C_r\phi\tau/2\pi s = \arctan \beta/\alpha$. Here C_r is the streamwise phase velocity of the traveling oblique waves, which was determined to be $0.4U_\infty$. Keeping the length of the wire-heater segments fixed, at a given phase velocity set by the free-stream speed, τ and ϕ could be adjusted to produce waves at any desired angle.

The plane TS wave input was produced separately by a single wire spanning the full width of the test section. This was individually controlled in amplitude, frequency and phase with respect to the oblique wave input. In most cases the TS and oblique modes were initially phase locked. However in some cases (Corke and Dal-Ferro, 1987) phase drift was allowed in order to see that effect on the resonance process. Generally, only exceedingly low seeding amplitudes of approximately 0.07 percent v'/U were

needed to promote subharmonic resonance, due to the perfect initial phase coherence of these modes. A single computer was used to provide the control signals to the heating wires, move velocity sensors, and to acquire voltage time series proportional to velocity. By this arrangement, the 3-D flow structures were fully phase locked in space and time, and thereby could be sampled by a single probe and reconstructed later by phase averaging. This involved multiple sensor probes capable of distinguishing separate velocity components.

The initial modes consisted of plane TS waves at a fundamental wave number $(\alpha,0)$, and subharmonic oblique waves of equal-opposite angles with wave numbers $(\alpha/2,\pm\beta)$. These were seeded with very low initial amplitudes and temporally phase locked. Inside Branch II, the TS mode amplified according to linear theory. The oblique modes, having a considerably higher minimum critical Reynolds number, were damped. When the plane TS mode reached sufficient amplitude, it interacted with the oblique modes, initially in the form of linear superposition. At this stage and throughout their development they were traveling at the same phase velocity. When the subharmonic oblique mode reached sufficient amplitude it gained further energy from the mean flow. At this stage, a basic change in the character of the subharmonic mode took place. This was seen as a movement of the subharmonic eigenfunction modulus maximum away from the wall to a point above the height of the critical layer, and an altering of the eigenfunction phase distribution from "wave-like" to "structure-like." Coincident with this was a similar change in the eigenfunction character of the initial fundamental wave prompting the growth of a new 3-D mode at the initial fundamental frequency. Throughout this metamorphosis, the phase velocities of these modes still remained the same as the initial TS mode.

The enhanced growth of the 3-D subharmonic mode produced other sum and difference modes which included $(3\alpha/2, \pm \beta)$, $(5\alpha/2, \pm \beta)$, $(\alpha, \pm 2\beta)$ and $(0, \pm 2\beta)$. The growth of these and their spatial character suggest a globally constant nonlinear energy transfer coefficient between them and the subharmonic mode.

The subharmonic mode continues to grow, but eventually saturates, and beyond that point decays. In this process, the modes nonlinearly phase locked with the subharmonic shift toward lower frequencies. Some of these were discreet modes such as the second subharmonic, $f/4$ $(f = C_r\alpha/2\pi)$. At this stage the velocity spectrum is quite broad-band, and the mean profile is more full indicating an increase in the viscous drag and a decrease in the shape factor. These characteristic changes first appear on the centerline of the subharmonic lambda structure, and eventually progress outward in span on the individual structures.

In the process of subharmonic mode growth, the two fundamental points of development were the location of maximum subharmonic amplification, and subharmonic energy saturation. The former marked the approximate location of the first appearance of 3-D modes in the flow visualization records. The location of these depended on the initial amplitudes of the seeded modes and on their streamwise and spanwise wave numbers. In one of our cases, these two points closely coincided. This was found to result in extra strong nonlinear phase locking with higher discreet modes.

What is the mechanism for subharmonic mode saturation? The evidence suggests there is a loss of precise phase locking between the subharmonic mode and higher interacted modes. This produced interactions such as $f/2 + nf/2 = nf$, where n has a value between 1 and 2. This, together with another documented interaction of $f/2 + f/4 = 3f/4$, provide a mechanism which acted to fill the spectrum on both sides of the fundamental frequency. These interactions, as well as others which were not sufficiently phase locked to appear as significant peaks in the cross-bicoherence estimates, would act to distribute energy in a broad band of modes. The mechanism for triggering the loss of precise phase locking may be the changes that occur in the mean flow produced as the subharmonic mode achieves larger amplitudes. One such change in the mean flow, produced by an interaction with the subharmonic was the mode $(0,\pm 2\beta)$.

This scenario of mode detuning prompted us to investigate conditions of non-fundamental/subharmonic resonance. This involved using a fixed streamwise frequency on the 3-D (oblique wave pairs) modes with different discreet frequencies on the plane TS mode, in the range from the exact fundamental up to 12 percent higher than the fundamental frequency. Examination of velocity spectra documented that in all these cases the same mechanism for resonant growth of 3-D modes existed, with some important differences. The fundamental/subharmonic mode detuning lead to numerous multiple interacted (sum and difference) modes. These spawned modes which would further interact with the primary subharmonic mode to produce third and higher generation offspring modes. This process lead to a rapid increase in the level of broad-band velocity fluctuations which quickly filled the spectrum. As the percentage of detuning was increased, the growth rate and maximum level of velocity fluctuations attained by the subharmonic mode decreased. However, the amount of energy in velocity fluctuations associated with other interacted modes more than compensated so that the overall level of fluctuation energy in coherent motions increased. The spanwise wave numbers of the interacted modes were traceable to the third harmonic, $\pm 3\beta$, of the primary 3-D mode with wavenumber, $\pm\beta$.

Cross-spectral analysis of time series taken at different x-locations with respect to a fixed reference located upstream of Branch II revealed the full picture of the nature of these interactions. For a situation with a 3-D mode input wave number $(\alpha_2, \pm\beta)$ and detuned plane TS mode with wave number $(\alpha_1,0)$ where $\alpha_1 = (2\alpha_2 + \Delta\alpha) > \alpha_2$, resonance in the strict sense of matched phase velocities was not possible, as in the case of the tuned condition $(\Delta\alpha=0)$. However, the 3-D mode interacts with itself to produce a tuned harmonic in the form $(\alpha_2,\pm\beta) + (\alpha_2,\pm\beta) = (2\alpha_2,\pm 2\beta)$. These have the same phase velocity. More importantly, these now act to mediate the nonlinear energy transfer to the other interacted modes at higher, lower and intermediate wave numbers. This process was revealed through third-order cross-spectral estimates. A comparison of these for the detuned cases show many similarities with the later stages of development of the initial tuned fundamental/subharmonic cases, supporting our initial hypothesis.

For the subharmonic resonance transition to turbulence, the method of "breakdown" is fundamentally different from that documented by Klebanoff et al. (1962) and referred here as K-type. Most notably the the change of phase velocity which occurred upstream of energy saturation, the high inflexional mean profile, the form of the y-eigenfunction phase distribution, and the

generation of large amplitude regular high frequencies past energy saturation, observed for K-type transition were not present here. For subharmonic transition, irregular higher frequency components are observable in the time traces when the subharmonic energy is sufficiently large and nonlinear behavior is evident. This can occur well upstream of subharmonic saturation and upstream of where the mean profile first deviates from Blasius. Some of these frequencies are attributable to sum and difference interactions with the subharmonic mode, as described earlier. The broadband frequencies begin to fill the layer starting from the wall and first appear at the cross-stream center of the lambda structure. By the point of subharmonic energy saturation, time traces on the centerline show broad-band frequencies at all parts of the subharmonic cycle, not just on the high velocity part as for the fundamental with K-type.

The basic difference between these two forms of transition is that for subharmonic transition, the resonant interaction between two modes allows an efficient mechanism for intercomponent energy transfer and early spectral broadening not present for fundamental mode (K-type) breakdown. By this approach the breakdown process can be explained through a nonlinear embellishment of spectral outgrowth due to secondary instability of basic modes rather than through higher order (tertiary or quartic) instability mechanisms. In this scenario, the flow does not "breakdown" but rather progresses through a natural sequence of sum and difference interactions which distribute energy at different spatial wave numbers leading to the smooth merging to a turbulent state.

II. TURBULENT BOUNDARY LAYERS STRUCTURE AND CONTROL

SUMMARY:

The events which are responsible for the majority of the turbulence production in the near-wall region of a bounded turbulent shear flow have been investigated in both a regular and a flat-plate manipulated boundary layer at high Reynolds numbers. The coherent structures associated with the bursting event were studied using the quadrant and shear-stress detection techniques. All three velocity components were measured in a three-dimensional sampling volume around the point of detection. The resulting pseudo-instantaneous representation of the 3-D flowfield conclusively demonstrates that a significant fraction of the turbulence-producing events are relatively large in scale, that a hierarchy of sizes exists, and that there is a link between the outer flow and the bursting process. It was also shown that strong sweeps of fluid towards the wall and ejections of fluid away from the wall can occur side by side, thus indicating a quasi-periodicity in the spanwise direction. The relation between the conditional structures and the long-time correlations demonstrate the importance of these structures in the dynamics and the turbulence production process of the boundary layer. All indications suggest that these scales are generated by a wall-layer mechanism but that a significant fraction of them gradually develop to sizes and convect with velocities scaling with the outer layer.

DISCUSSION:

Previous studies concerning the scaling of burst frequency with Reynolds number have been performed at a constant y^+ using a single detection technique. The present results are more thorough in the sense that measurements were performed from y^+=15 to 220 using u-level, VITA & quadrant detection schemes over a wide range of Reynolds numbers; $3000 < Re_\theta < 10400$. The correct scaling of the frequency of ejections and bursts was found to be very sensitive to spatial-averaging effects. The ejection, sweep, inrush and bursting frequencies were determined to scale with inner variables for all y^+ values used, only after proper correction for sensing-length effects was performed.

The distinction between frequency of ejections and bursting frequency has helped to understand the role that manipulators have on the bursting process in the near-wall region. For a flat-plate manipulated boundary layer (resulting in net drag reduction), the frequency of ejections was observed to increase by three percent; however, the bursting frequency was seen to decrease by seven percent.

The effects of manipulators, placed at relatively large y/δ (y/δ_m = 0.8), on the coherent structures are in agreement with the above mentioned bursting results. The reduction in the spanwise extent of the coherent structures of approximately 10% is consistent with the 7% decrease in bursting frequency. Specifically, the manipulators placed at high y/δ are assumed to affect only the largest of the coherent structures; therefore, a moderate decrease in spanwise extent is expected. In addition, the placement of the blades at lower y^+ values resulted in an increased reduction in the spatial extent and frequency of events. These results tend to support the conclusion that the ensemble-averaged coherent structure represents a collection of events of varying size and that a link between the outer flow and the bursting process exists.

The results of the present investigation have resolved many of the key issues concerning the large-scale coherent structures in a turbulent boundary layer. In many general and detailed aspects the results are in excellent agreement with those of Guezennec (1985); thereby confirming his calculation of w from the measured u and v. It appears, however, that his supplementary τ_z condition for detecting events is unnecessary for the high threshold used on τ_z; at least for the ensemble-averaged results.

The coherent structures associated with the turbulence production process were studied, with the aid of the quadrant and wall-shear detection techniques, through measurements of all three velocity components in a three-dimensional sampling volume around the point of detection. By constructing pseudo-instantaneous conditional probability density distributions at all sampling points, it was conclusively demonstrated that a significant fraction of the individual events associated with the bursting process are large in scale. That is, the ensemble-averaged representation is indeed an accurate portraiture of the flowfield associated with bursting and is not simply an artifact of the conditional averaging. The larger scales were found to extend outward to $y^+ > 600$, have a spanwise extent on the order of 600 wall units, and persist for several δ in the streamwise direction. Strong sweeps and ejections of fluid were shown to occur side by side at

least 15% of the time indicating a quasi-periodicity in the spanwise direction of strong turbulence-producing events. This quasi-periodicity is most significant to the phenomenological models of wall layers. The three-dimensional representation of the probability density distributions further points to a hierarchy of scales associated with the turbulence-production process.

The quadrant detection scheme was compared with the shear-stress detection scheme in a regular boundary layer. The results for a condition of high streamwise shear stress at the wall was found to agree well with the Q4 detection scheme. However, the events associated with a large negative value of the fluctuating streamwise shear stress were not observed to be as highly correlated with Q2 events; i.e, primarily in the streamwise perturbation velocity. Regardless, it was determined that the shear-stress technique detected the large structures associated with the turbulence production process as well as, if not better than, the quadrant detection scheme.

The percentage of events used in the conditional-averaging process and for the development of the pdf's compared with those "visually observed" was found to be approximately 40%. This fact and the relation of the coherent structures to the space-time correlations lend support to the argument that these structures are the coherent structures of the boundary layer. Specifically,the convection velocities inferred from both the long-time correlations and the conditional probability density functions are equivalent. They were determined to convect at speeds slightly greater than the local mean velocity, but less than the free-stream velocity. More importantly, the frequency of occurrence of these events is relatively small; however, the long-time correlations are dominated by the influence of the structures. All indications suggest that these scales are generated by a wall-layer mechanism but a significant fraction of them gradually develop to sizes and convect with velocities scaling with the outer layer.

The large amount of data taken for the present study has not been exploited to the fullest extent and can be reprocessed using the various detection schemes to determine the relation between them. For example, the strong Q2 and Q4 events were not seen to occur in rapid succession; however, the VITA event has been shown by Guezennec (1985) to be made up of a Q4 followed by a Q2. The 3-D probability distributions can be recalculated using VITA as the detection function, with various thresholds on the Q2 and Q4 events occurring within the sampling domain. The exact relation of the VITA event to the turbulence-producing events detected by the quadrant method, as well as its spatial description, could then be determined.

The three-dimensional conditional probability distributions have proven to be a very powerful tool in understanding the events associated with the bursting process. One major question which still remains is that of the instantaneous symmetry of these events with respect to the point of detection. By using two mapping X-wire probes in addition to the detection sensors, one can do conditional pdf's between not only the detection point and various points in space, but also between the sampling positions located symmetrically on either side of the detection point. These 3-way conditional pdf's will answer the instantaneous symmetry question for a relatively high Reynolds number boundary layer.

III. MANAGEMENT OF UNSTEADY AND THREE-DIMENSIONAL SEPARATED FLOWS

SUMMARY:

The following discussion describes the overall directions and goals of research work on the management and control of unsteady separated and vortical flows, to be carried out at the Fluid Dynamics Research Center. The statement also describes some specific experiments that are being carried out as part of these investigations. The work described herein is a natural outgrowth of the investigations carried out at the FDRC under contract for the AFOSR (Contract F49620-84-C-0080), and enlarges upon these investigations in light of results from recent investigations at the FDRC.

DISCUSSION:

We plan to pursue investigations in several specific areas described below. The overall objectives are to develop the techniques and capability for the prevention or control of separated flows, particularly under unsteady operating conditions, and the control of unsteady forces and moments on various configurations.

The facilities of the FDRC include the capability to generate controlled time-varying flow fields (in both the A.A. Fejer wind tunnel and the National Diagnostic Facility) and to map flow fields with a variety of tools including the two-component LDA, tomographic flow visualization, scanning LDA, multi-probe hot wire systems and Scanivalue pressure systems. Together with the sophisticated data acquisition and presentation capabilities available at the center, they provide a unique infra-structure that facilitates this program of work.

A. Active control of separated flow about airfoil geometries

Current experiments to obtain reliable pressure signatures of separation (or incipient separation) in unsteady flow fields over basic geometries are yielding results that will help identify appropriate indicators of flow state in an unsteady separated flow. The results from these experiments will be used to examine the feasibility of active control of separated flows over airfoil geometries in pitching motion. The study will focus initially on a 2D symmetric airfoil but will be extended to 3D geometries. (The latter will include delta wings and finite swept wings at an angle of attack.) A variety of approaches to effect the control will be investigated, including suction, leading edge flaps and slats, and techniques to introduce transverse or streamwise vorticity in the flow field at appropriate points. In addition, the unsteady forcing technique described in (B) below will also be explored (as a means of controlling the base flow region). A natural extension of the active control experiments will be to investigate the possibilities of reactive control with feedback.

B. Unsteady, zero mass base bleed

Experiments at IIT have demonstrated the effectiveness of the unsteady base bleed technique for modifying the flow around bluff bodies. This method uses unsteady pulsating jets with zero net mass addition to

modify the flow field. The effectiveness of the technique has been demonstrated on the wake behind circular cylinders for flow at low Reynolds numbers. At the proper frequency and amplitude, the wake momentum thickness was reduced to zero which means the drag has been essentially eliminated.

The unsteady base bleed technique is attractive from the design standpoint because no net mass is added to the flow, and the body itself does not move. This means it is not necessary to carry a supply of bleed fluid, or pay any drag penalty associated with suction ports. Furthermore, the unsteady base bleed can be turned on and turned off as desired, and variations in frequency and amplitude cause variations in the level of control. In this way it is possible to tailor the amount of flow control with the unsteady base bleed technique.

In order to make the unsteady base bleed technique useful for the aircraft designer, we must learn more about the physical mechanisms and parameters governing the interaction between the base bleed and the separated flow. We are undertaking the following four tasks to achieve these goals.

1) Develop higher frequency and stronger amplitude forcing mechanisms capable of exerting control in high-speed flows.

2) Conduct a parametric study to determine the scaling parameters necessary to design practical control systems. In addition we will define the "control envelope" (freq-amplitude, Re) for the steady flow elliptical forebodies (described in C).

3) Apply the unsteady technique to the pitching forebody problem. The unsteady base bleed technique will modify the flow at high angles of attack, but may lose this ability at lower values.

4) Apply the unsteady base bleed to the control of airfoil wakes as described in A. In particular, the technique will be used to reduce the drag and level of turbulence associated with the wake of the airfoils. The method will be tested on both steady and pitching airfoils.

C. Unsteady Vortex System About Axisymmetric slender body/forebody geometries

Experiments are now underway to examine the unsteady flow about a slender body of circular cross section with a conical forebody, as it undergoes an unsteady motion. By increasing the major/minor axis ratio (aspect ratio) of cylinders with elliptical cross-sections, we can observe the change in the vortex structure as the geometry changes from a circular cylinder to a flat plate.

The elliptical cross-sections are closer approximations to modern aircraft forebodies, and we expect to find more complex flow behavior during a pitching motion than with the simple circular cylinder. For example, the boundary layers attached to the different geometries will experience different development histories before reaching the

separation line. Certainly different regimes of vortex behavior such as a steady system of vortices or unsteady shedding will be encountered as each body pitches. The tomographic flow visualization currently under development will be used to map the different regimes. An attempt will be made to collapse the data on the basis of aspect ratio. Quantitative information are obtained when necessary using LDA measurements.

D. Canard Vortex-Wing interaction studies

In modern aircraft with canards, the vortex that is shed from the canard tip may interact with the aircraft wing. It may be possible to control the position of this longitudinal vortex with an active feedback control loop. Potential benefits from controlling the position of this vortex would be more stable aircraft performance, enhanced lift and roll moments. With the experience at IIT in the area of vortex-surface interaction and with the techniques developed for generating streamwise vorticity, we are in an ideal position to pursue active feedback loops for controlling the trajecteries of the Canard-tip vortex.

It is proposed to generate a streamwise vortex (primary vortex) with controllable strength in the central part of a wind tunnel. A two-dimensional control wing will deflect the primary vortex downward, so that it interacts with a flat plate in the wind tunnel.

It is well known that the trajectory of the primary vortex is not accurately predicted by inviscid theory when the vortex approaches a solid boundary, because a secondary vortex is induced which alters the path of the primary vortex. The location of the primary vortex will be determined instantaneously with an array of pressure sensors connected to a computer. Depending on the pressure gradient developed by the vortex, the computer will select specific suction ports in the floor of the wind tunnel to be activated. The suction ports will generate a counteracting pressure gradient that will remove the induced vortex, thereby modifying the trajectory of the primary vortex. By changing the angle of attack of the control airfoil it will be possible to change the approach angle and spanwise position of the primary vortex. By pitching the control airfoil an unsteady motion of the primary vortex can be established that will allow the active control loop to be tested. If the active control is effective, then it should be possible to "freeze" the trajectory of the primary vortex, even in the case of the unsteady motion generated by the control airfoil.

E. Wing-body junctions

Strong streamwise vortices are known to form in the corner flows formed by wing-body junctions. When these vortices separate from the body, they may adversely affect on the performance of the aircraft. It is proposed to examine two generic cases consisting of delta wings combined with an elliptical cross-section cylinder and with a circular cylinder. Each geometry will be examined with three-dimensional flow visualization to determine the vortex system that is established. The dependence of the vortex system on angle of attack and pitching rate will be examined. Depending on the results of other experiments, a specific control technique will be chosen to modify the vortex flow field.

IV. SCANNING LASER ANEMOMETER

SUMMARY:

A forward-scatter laser anemometer has been modified with the use of optical scanners and a laboratory mini-computer to allow the rapid scanning of the probe volume. The scanning laser anemometer measures one component of velocity at locations in a plane parallel to the probe volume fringes. For the case when scanning rates are much faster than the rate of change of the flow field, then a quasi-instantaneous map of the flow field is obtained. The scanning system has excellent spatial resolution and can capture the details of transient flow events without the use of conditional sampling techniques. Real-time display of the velocity field is provided on the computer display.

DISCUSSION:

Very often it is necessary to obtain spatial correlations, wavenumber, phase distributions or other spatial quantities in order to describe the spatial character of disturbances found in both laminar and turbulent flow fields. For example, symmetric-antisymmetric mode competition in wakes, secondary instability in jets, wakes and boundary layers, and coherent structures in turbulent flows require spatially detailed information in order to be accurately described. However, it is difficult to obtain spatial information with stationary, single-point measuring techniques like the hot-wire anemometer and laser anemometer. Basically, one has the choice of constructing rakes of probes, using a flying hot-wire or using some type of conditional sampling technique. The first two choices tend to disturb the flow and rakes of probes have limited spatial resolution. All conditional sampling techniques require averaging, which "smears" the event to be detected. The scanning laser anemometer attempts to overcome these limitations by its nonobtrusive nature and its ability to sample an area in the flow at very high speed. Provided a region in space can be sampled much faster than the rate of change of the flow field, then a quasi-instantaneous velocity map can be obtained. From this data base the spatial correlations, spatial phase, spectra, etc. may be computed.

The design of the scanning laser anemometer is an extension of the system developed by Chehroudi and Simpson(1984). The new design is capable of scanning in two directions, i.e., along the optical axis and perpendicular to it, in order to sample over a plane in the flow. An argon-ion laser beam (1.4W at 514.5nm) is split into two beams, one of which is frequency shifted by a 40 MHz acousto-optic modulator, BC. The stationary prisms P1, P2 and mirrors M1, M2 steer the beams to a wider angle. The first optical scanner, SM1, controls sampling volume position along the z-axis (out of the page). The optical scanners SM2 and SM3 control the beam intersection angle, and position of the probe volume along the optical axis (y-axis). The beams are blocked on the backside of the water channel test section by the mask MS1. The light scattered from the 2um seeding particles is imaged on a photomultiplier tube, PM, by two cylindrical lenses, RL1 and RL2. Additional details of the optical components of the system can be found in the thesis by Economou(1986).

The signal from the photomultiplier is processed by a TSI model 1990-C counter. Typical data rates at the counter range between 4kHz and 5kHz with signal downmixing at 50kHz. The data-ready pulse from the counter triggers a series of clocks on a Masscomp computer. The data acquisition system acquires the scanner position signals, counter frequency, exact time of measurement and any additional data through the a/d converter and parallel interface. Scanner motion is controlled by the d/a output from the computer. The data is processed by an array processor and displayed in real time on a graphics terminal display. The "instantaneous" velocity field, mean and rms velocity are shown simultaneously on the display. This feature is particularly useful during experiments with flow control techniques, since the experimenter can observe the velocity field as changes are being made and quickly assess the effects of the control on the flow field.

The majority of the work at IIT has been with a water channel, although some preliminary measurements have been conducted in air. The probe volume scans over 9cm along the optical axis and 5cm perpendicular to the optical axis in the z direction. Typical scanning rates have been between 10 and 20 scans/sec. Although it is possible to scan much faster, the noise level associated with the scanning increases as the square of the scan rate. To get a rough idea of the level of noise in the system, a typical freestream velocity of 4cm/sec and a scanning rate of 20 scans/sec generates a noise level of approximately 1.5 percent of the freestream velocity. We expect to be able to reduce the noise even further by improvements in the mounting system for the scanners.

In addition to the noise level dependence on the scanning rate, both the temporal and spatial resolution are affected by scanning. When scanning along a line one obtains a measure of the instantaneous velocity profile with each scan, thus the scan rate becomes roughly analogous to a profile sampling rate. Obviously, the higher the scan rate, the better the temporal resolution. However, the spatial resolution is coupled to the scan rate, and it tends to decrease as the scan rate increases. Doubling the scan rate would increase the average space between measurements, and would tend to decrease the data rate at the counter as well. Therefore, all of these parameters must be carefully considered when designing an experiment with a scanning laser anemometer. In our experiments on controlling the formation of the Karman vortex street, the scan rate was 20 scans/sec. The data rate at the counter was approximately 4kHz and the scan length was 9cm. This amounts to an average spacing between measurements of 0.9mm. For comparison, one would need to place 100 individual probes in the flow to obtain the same spatial range and resolution.

The scanning laser anemometer system has been used successfully to make multiple-point, quasi-instantaneous measurements in wakes behind bluff bodies and in highly unsteady, pulsating jets. The system offers good temporal/spatial resolution over a wide range in the flow. The use of the scanning system played a major role in the development of the zero-mass base bleed technique. Our efforts are currently focussed on developing new software to acquire and display the data during scanning over an area. Furthermore, some effort needs to be spent on development of new data processing techniques to describe the two-dimensional fields of data already acquired while scanning over a line.

V. REFERENCES

Chehroudi, B. and Simpson, R. L. 1984. A rapidly scanning laser Doppler anemometer. J. Phys. E, 17, pp.131-136.

Corke, T. and Mangano, R. 1987. Transition of a Boundary Layer: Controlled Fundamental-Subharmonic Interactions. Proceedings of the Symposium on lent TurbuManagement and Relaminarization, Bangalore, India, Published by Springer-Verlag, p. 199.

Corke, T. and Mangano, R. 1987. Transition of a Boundary Layer: Controlled Fundamental-Subharmonic Interactions. IIT Fluid Dynamics Center Report 87-1. (Submitted to JFM)

Corke, T. and Dal-Ferro, P. 1987. Later Stages of Transition in Three-Dimensional Seeded Boundary Layers. IIT Fluid Dynamics Center Report 87-2. (Manuscript in preparation for JFM)

Craik, A. D. D., 1971. Nonlinear resonant instability in boundary layers. J. Fluid Mech. 50, p. 393.

Economou, M. 1986. Design and Analysis of a Scanning Laser Anemometer. M.S. Thesis, Illinois Institute of Technology.

Guezennec, Y. G. 1985. Documentation of Large Coherent Structures Associated with Wall Events in Turbulent Boundary Layers. Ph.D. Thesis, Ill. Inst. of Tech., Chicago, IL.

Herbert, Th., 1983. Subharmonic Three-Dimensional Disturbances in Unstab.e Plane Shear Flows. AIAA paper 83-1759.

Klebanoff P. S., Tidstrom, K. S. and Sargent, L. M., 1962. The Three-dimensional Nature of Boundary-layer Instability. J. Fluid Mech. 12, p. 112.

Nagib, H. M., Wark, C. E. and Guezennec, Y. G. 1987. Documentation of Turbulence Producing Structures in Regular and Manipulated Turbulent Boundary Layers. Proceedings of the IUTAM Sumposium on Turbulence Management and Relaminarisation. Bangalore, India. Springer-Verlag, Paper#1.

Nagib, H. M. and Guezennec, Y. G. 1986. On the Structure of Turbulent Boundary Layers. Proceedings of the 10th Symposium on Turbulence, Rolla, Missouri, paper #1.

Wark, C. E. 1988. Experimental Investigation of Coherent Structures in Turbulent Boundary Layers. Ph. D. Thesis., Ill. Inst. of Tech., Chicago, IL.

Wark, C. E. and Nagib, H. M. 1988. On the Character of Turbulent-Producing Events in Near-Wall Turbulence. Zoran Zaric Memorial International Seminar on Near-Wall Turbulence, Dubrovnik, Yugoslavia.

END

DATE

FILMED

DTIC

10-88